

Manuscript Number:

Title: A Double Safety Lock Tumor-Specific Device for Suicide Gene Therapy in Breast Cancer

Article Type: Original Research Article

Keywords: Elastin-like recombinamers (ELRs)
nanocarriers
polyplex
suicide gene therapy
breast cancer

Corresponding Author: Dr. Francisco Javier Arias,

Corresponding Author's Institution: University of Valladolid

First Author: Maria J Piña, PhD

Order of Authors: Maria J Piña, PhD; Alessandra Girotti, PhD; Sofia Serrano-Ducar; Raquel Muñoz; J. Carlos Rodríguez-Cabello; Francisco Javier Arias

Suggested Reviewers: Abhay Pandit
National University of Ireland NUI Galway
abhay.pandit@nuigalway.ie
He has done very interesting contributions in the fields of functional biomaterials and targeted controlled-drug-release systems

Joao Mano
University of Aveiro
jmano@ua.pt
Due to his experience with nanotechnology approaches applied to natural-derived biomaterials in order to obtain biomedical devices with improved structural and multifunctional properties, to control cell behaviour and organization, to be used in therapies.

Ashutosh Chilkoti
Duke University
chilkoti@duke.edu
His research is focused on applications including the delivery of anticancer therapeutics to solid tumors by self-assembled nanoparticles of Elastin Like Polymers-drug conjugates

A Double Safety Lock Tumor-Specific Device for Suicide Gene Therapy in Breast Cancer

Corresponding author: F. Javier Arias

Other authors: Maria J. Piña, Alessandra Girotti, Sofía Serrano, Raquel Muñoz, J. Carlos Rodríguez-Cabello

Type of manuscript: Article

Significance:

In this work, we described a novel selective nanodevice able to eliminate tumor cells while leaving healthy ones intact. To achieve this objective, a carrier in the form of a polyplex with therapeutic DNA, was tested. This carrier forms a double-lock multifunctional device due to specific binding to a tumor cell marker and the selective expression of therapeutic DNA inside human breast-cancer cells. The therapeutic efficiency of the double-lock device was evaluated by way of in vivo assay. Inhibition of tumor progression was detected early and found to be very significant at the end point, with a dose-dependent reduction in tumor mass being observed. These results represent an important step toward the rational development of an efficient, safe and more specialized gene-delivery device for tumor therapy. Novel drug delivery shuttles and gene delivery are some of the most interesting topics for *Cancer letters*, so in our opinion this work is suitable for its publication in *Cancer letters*.

Reviewers:

In our opinion, **Abhay Pandit** (abhay.pandit@nuigalway.ie), from National University of Ireland NUI Galway, could be a proper reviewer, as he has done very interesting contributions in the fields of functional biomaterials and targeted controlled-drug-release systems. We also recommend **Joao Mano** (jmano@ua.pt), from University of Aveiro, due to his experience with nanotechnology approaches applied to natural-derived biomaterials in order to obtain biomedical devices with improved structural and multifunctional properties, to control cell behaviour and organization, to be used in therapies. Finally, we recommend **Ashutosh Chilkoti** (chilkoti@duke.edu) from Duke University as reviewer, as his research is focused on applications including the delivery of anticancer therapeutics to solid tumors by self-assembled nanoparticles of Elastin Like Polymers-drug conjugates.

The manuscript has not been published previously by any of the authors and is not under consideration for publication in another journal at the time of submission.

All authors have seen and approved the submission of the manuscript.

Highlights:

- The biocompatibility of the novel non-viral vector construct for the target cancer cells was confirmed.
- The aptamer binds to the aberrantly hypoglycosylated MUC1 located on the breast cancer-cell surface.
- Treatment of mice bearing breast tumors with therapeutic polyplex decreased tumor volume.
- The reduction in tumor volume was confirmed by weighing the tumors post-necropsy.
- The treatment acts in a specific and selective way on tumor cells, as demonstrated by evaluating the prognostic factors.

ABSTRACT

The complexity and continuous evolution of cancer make the design of novel strategies of treatment a constant challenge in biomedicine. Moreover, most of cancer treatments are still not tumor-specific and provoke high systemic toxicity. Herein we have developed a novel selective nanodevice to eliminate tumor cells while leaving healthy ones intact. To achieve this objective, a polyplex carrier, comprising an elastin like-recombinamer covalently conjugated to an aptamer and complexed with therapeutic DNA, was tested. This carrier forms a double-lock multifunctional device due to specific binding to a tumor cell marker and the selective expression of therapeutic DNA inside human breast-cancer cells. Due to the stability provided by ELRs, the homogeneous population of polyplexes obtained showed selective toxicity against cancer cells in in vitro and in vivo assay. Inhibition of tumor progression was detected early being very significant at the end point, with a dose-dependent reduction in tumor mass. Histological studies revealed a specific reduction in tumor parenchyma and in specific tumor cell markers. These results represent an important step toward the rational development of an efficient, safe and more specialized gene-delivery device for tumor therapy.

TITLE: A Double Safety Lock Tumor-Specific Device for Suicide

Gene Therapy in Breast Cancer

Maria J. Piña, Alessandra Girotti, Sofía Serrano, Raquel Muñoz, J. Carlos Rodríguez-Cabello, F. Javier Arias*

BIOFORGE (Group for Advanced Materials and nanobiotechnology), CIBER-BBN, University of Valladolid, Valladolid, Spain.

*Corresponding author: arias@bioforge.uva.es

1. INTRODUCTION

Breast cancer is the most commonly occurring cancer diagnosed in women in Western societies, with men also being affected but to a lesser extent. Despite considerable recent progress in the early detection of breast cancer and the improved treatments, such as immunotherapy, chemotherapy, radiotherapy or endocrine therapy available, which have been shown to improve the clinical outcome, the cure rate has not increased and mastectomy is often also required, thus causing significant psychological sequelae in affected patients [1]. Moreover, chemotherapy and radiotherapy treatments are not cancer-specific and also present side effects that often imply a worsened condition and increased patient discomfort. This situation suggests the need to develop new alternative therapeutic approaches, such as gene therapy, that may prove useful alone, or in combination with existing ones, as regards focusing treatment only at the site of action to ensure increased effectiveness, reduce the treatment dose, and decrease adverse systemic side effects [2, 3]. In addition, gene therapy offers the possibility of treatments that eradicate tumors without damaging normal tissue [4]. Different approaches have been developed in gene therapy to treat breast cancer, including the transfer of toxic or pro-apoptotic genes. To date, most research into suicide gene

therapy in breast cancer has focused on the use of viral vectors [5-9], mainly due to their higher transfection levels. Thus, herpes simplex virus thymidine kinase (HSVtk) gene has been delivered by an adenovirus in combination with ganciclovir as the first and most common strategy used in experimental and clinical studies of suicide gene therapy [10, 11]. However, recent promising advances in the field of non-viral vectors represent a real alternative in terms of safety and cost-effectiveness [12, 13]. Several non-viral systems have been applied for suicide gene therapy purposes as well to carry therapeutic plasmids controlled by tumor-specific promoters. The latter allow the gene of interest to be selectively expressed in cancer cells without damaging healthy ones [14]. Human epidermal growth factor receptor 2 (HER-2) [15], survivin [16] or mucin-1 (MUC-1) [17] promoters have been used to control the expression of suicide genes. MUC1 is a transmembrane glycoprotein which is overexpressed and aberrantly glycosylated in many epithelial cancers, such as pancreas, lung, colon, prostate and breast cancers [18,19]. Cancer-associated post-translational glycosylation pattern determines the incomplete glycosylation of MUC1 forms. Hypoglycosylated MUC1 forms are expressed only in cancer cells and therefore, they are of great interest as immunotherapy targets and prognostic biomarkers. For instance, the MUC1 promoter was shown to control expression of the targeted truncated proapoptotic tBid gene delivered by poly(ethylene glycol) (PEG)-polyethylenimine (PEI)-based polyplexes in breast cancer cells [17]. In addition, tumor-specific promoters provide a safe and effective strategy for designing gene-therapy systems that can be adapted for use with various tumors or delivery systems. To date, ELRs and other polymers widely used as non-viral vectors, such as poly-lysine (PLL), polyethylenimine (PEI), polyethyleneglycol (PEG), chitosan, poly(lactic-co-glycolic acid) (PLGA), or poly(2-dimethylaminoethyl methacrylate) (pDMAEMA) [20], have found increasing applications in biomedicine due their

inherent biocompatibility and smart properties [21-29]. A previous study showed the ability of ELRs joined to functional peptides to be used as delivery vectors with no cellular effects *in vitro* [30]. Further research with ELR-based polyplexes coated with MUC1-specific aptamers opened the way to the use of ELRs part of a breast cancer selective vector [31]. MUC1, which is known to be aberrantly overexpressed in about 90% of breast cancer cells, was used as targeting glycoprotein by the 5TR1 aptamer [32]. The ribosome inactivating protein (RIP) type I Pokeweed antiviral protein (PAP-S) has also been tested as a suicide gene and found to induce higher cell death in target transfected cells in comparison with controls [31].

Conversely, it is important to note that type 1 RIPs are not as toxic as type 2 RIPs since they are unable to cross the cell membrane on their own. Despite the high amounts of toxin produced, death events were only induced in transfected cells, in other words there is a greater possibility of generating an immune response and a dependence on the transfection efficiency, thereby limiting their potential of suicide therapy. In order to increase the harmful potency of the suicide gene, the type II RIP ricin, which is produced naturally by *Ricinus communis*, is proposed in the present study [33, 34]. Ricin is synthesized as preproricin, which comprises a 24-amino-acid N-terminal signal sequence followed by the A chain, which is attached to the B chain by a 12 amino-acid linker [35]. During synthesis, the signal sequence is removed to generate the mature protein, in which chains A (N-glycosidase activity) and B (lectin which binds to β -1,4-linked galactose residues) are bound by a disulfide linkage. When chain A is bound to chain B, the latter allows rapid internalization into the cell and translocation of the catalytic chain to cytoplasm, thus triggering inactivation of the 28S RNA in the 60S ribosomal subunit [36] and inhibiting protein synthesis, thereby leading to cell death. Ricin-induced apoptosis mediated by different caspases, depending on the cell type, has

been also described in *in vitro* studies [37-39]. Most of the research into ricin has been performed in cancer immunotherapy using chain A or blocking the galactose-binding sites from chain B [40]. The results showed the ability of these immunotoxins to kill human myeloma, lymphoma and lung cancer cells, amongst others [41-44]. A phase I clinical trial with “Combotox”, which is a mixture of two immunotoxins prepared by coupling deglycosylated ricin A chain (dgRTA) to monoclonal antibodies targeting CD22 (RFB4-dgRTA) and CD19 (HD37-dgRTA), showed complete remission in three of 17 patients with acute lymphoblastic leukaemia (ALL) [45, 46]. However, the whole ricin protein has not been used *in vivo* due to the high cytotoxicity levels induced by ricin holotoxin. Compared with conventional agents, ricin has some features, such as a potent action, an inability to induce resistance and the fact that it can act on both dividing and non-dividing cells that make it attractive, although side effects such as vascular leak syndrome or demyelination, have to be controlled. To date, no suicide therapy studies using ricin gene to combat breast cancer have been conducted.

In this study we developed a complete delivery system comprising two elements, namely a transfection vector and therapeutic DNA content. To obtain the transfection vector, the polycationic ELR (VPGKG)_{x72} [31] was covalently linked to the 5TR1 aptamer by means of click chemistry [47]. This aptamer is known to be directed towards the underglycosylated variable number tandem repeat (VNTR) region of MUC1, which is rich in serine, proline and threonine, and has previously been designed and used for molecular targeting [48, 49]. Moreover, the therapeutic DNA was designed to contain the MUC1 tumor specific promoter (hMUC1 promoter) and ricin gene modified with the preprotrypsin leader sequence. The use of preprotrypsin leader should allow the secretion of mature ricin and its diffusion from the transfected tumor to neighboring cells, thus triggering the bystander effect [50]. Both the vector and therapeutic DNA

constitute a double safety lock device controlled by the presence of MUC1 on the cell surface and applied to directed suicide therapy for breast cancer *in vitro* and *in vivo*. This article reports the effective inhibition of tumor growth in mice treated with ELR-5TR1 pDhMUC1-ricin polyplexes.

2. MATERIALS AND METHODS

2.1. Chemicals, proteins and cell lines

Unless otherwise indicated, all chemicals were purchased from Sigma Aldrich (Germany). Restriction and modification enzymes for DNA cloning were purchased from Thermo Fisher (USA). TNHS-PEG-cyclooctyne was purchased from SynAffix (ref. SX-A1006, Netherlands). The preproricin gene was purchased from NZYTECH (Portugal) and the pDrive5Lucia-hMUC1 plasmid, abbreviated as pDhMUC1-luciferase, from Invivogen (USA). Paraformaldehyde and Turbofect were purchased from Sigma Aldrich (Germany).

The fluorescent labelled aptamers 5TR1-Cy5.5 (5'Cy.5.5-GAAGTGAAAATGACAGAACACAACA-Azide'3) and 5TR1 (5'-GAAGTGAAAATGACAGAACACAACA-Azide'3) were purchased from Metabion (Germany). Reagents for histological analysis were purchased from Sigma and antibodies were purchased from Abcam (UK), unless otherwise indicated.

XL-1 Blue competent cells (ref. 200249) were purchased from Stratagene (USA). Human foreskin fibroblasts HFF-1 (ref. SCRC-1041) and human breast adenocarcinoma SKBR3 cells (ref. HTB-30TM) were purchased from the American Type Culture Collection (ATCC, USA). Human breast cancer MCF-7 (ref. 86012803) and liver hepatocellular carcinoma HepG2 (ref 85011430) cell lines were supplied by Sigma-Aldrich. Basal medium Dulbecco's modified Eagle's medium (DMEM),

Eagle's minimum essential medium (EMEM), McCoy's 5A medium, 2mM glutamine, and 1% NEAA, fetal bovine serum (FBS), penicillin streptomycin solution, trypsin-EDTA, DPBS, LIVE/DEAD® Viability/Cytotoxicity Kit for mammalian cells, and Alamar Blue® were supplied by Invitrogen (USA).

2.2. Design and cloning of pDhMUC1-ricin plasmid

The therapeutic plasmid pDhMUC1-ricin was obtained by replacing the luciferase gene with the modified ricin gene in the original pDhMUC1-luciferase plasmid. The ricin gene was cloned downstream of the preprotrypsin leader-ricin gene using *NcoI* and *NheI* restriction enzymes. The XL-1 Blue competent *Escherichia coli* strain was transformed with the recombinant plasmid and grown in agar medium containing the selection agent zeocin (Invivogen, USA). The sequence correctness of the recombinant vector was confirmed by diagnostic digestion using the *EcoRI* restriction enzyme and followed by DNA sequencing. All plasmid DNAs (pDNA) were purified using the Endofree® Plasmid Maxi Kit (Qiagen, Germany).

2.3. Synthesis and characterization of the transfection vector (ELR-5TR1)

2.3.1. Preparation of ELR-PEG-cyclooctyne

ELRx72 (abbreviated as ELR) was biosynthesized as described by Piña *et al.* [31]. Thus, 1 equivalent of ELR (20 mg/mL) dissolved in dimethyl sulfoxide (DMSO) was mixed with 0.46 equivalents of NHS-PEG-cyclooctyne (3 mg/mL) in DMSO under a nitrogen atmosphere at 37°C. The mixture was stirred overnight at 25°C. After this time 30 mL of fresh ultrapure water was added to the crude mixture, dialyzed against water and lyophilized. The incorporation of PEG into the ELR as ELR-PEG-cyclooctyne was evaluated by nuclear magnetic resonance (NMR).

2.3.2. Preparation of ELR-5TR1

1.1 equivalents of azide-5TR1 aptamer or the fluorescent version azide-5TR1-Cy5.5 (10 mg/mL) were mixed with one equivalent of ELR-PEG-cyclooctyne (10 mg/mL) previously dissolved in ultrapure water and the resulting mixture incubated at 4°C for 48 hours. After this time the product was dialyzed against ultrapure water at 4°C and lyophilized. Incorporation of the aptamer was corroborated by gel retardation assay and quantified by absorbance spectrophotometry (at 260 nm) and flow cytometry.

2.3.2.1. ELR-5TR1 characterization: Electrophoretic mobility shift assays (EMSA) and spectrophotometry assay

ELR-5TR1 was dissolved in ultrapure water at 1 mg/mL and treated with 10% SDS, then submitted to electrophoresis on 3% MetaPhor™ agarose (Lonza, USA) gel in 1xTAE buffer at 6 V/cm, staining with SimplySafe™ (EURx, Poland). 5TR1 aptamer was used as control. The conjugated oligonucleotide was visualized by exposure to UV light in a transilluminator (Vilber, Germany). ELR-5TR1 was dissolved in ultrapure water at 1 mg/mL and absorbance was measured at 260 nm using a Nanodrop 2000 instrument (Thermo scientific).

2.4. Preparation of polyplexes

Polyplexes comprising ELR-5TR1-pDNA were formed at a 50/1/4 ratio in aqueous solution (N/P/P_{apt}, where N corresponds to the number of amine groups from the polymer, P to the phosphate groups from the plasmid DNA and P_{apt} to the phosphate groups from the aptamer). Adjustment to the 50/1/4 ratio was achieved by mixing both ELR-5TR1 and free ELR. To prepare the polyplexes, ELR-5TR1 biopolymer was previously dissolved overnight in 5% glucose (w/v) solution to a concentration of 1 mg/mL at 4°C. Complexes were formed by mixing the pDNA with

the ELR solution. The mixture was vortexed vigorously at 25 °C for 1 minute and then incubated at 25 °C for 30 minutes to allow polyplex formation.

2.4.1. Polyplex characterization by flow cytometry

Polyplexes with the fluorescent labelled aptamer 5TR1-Cy5.5 were formed and characterized by flow cytometry. ELR-5TR1-Cy5.5-pDNA polyplexes were formed in aqueous solution. The incorporation of 5TR1-Cy5.5 was evaluated using a Gallios flow cytometer (Beckman Coulter, USA) with the side-scatter outcome set to logarithmic. A flow rate of 75,000 events/s was recorded, with a total of 100,000 events per measurement. Data were analyzed using Flowing Software.

2.5. Physical characterization of polyplexes

2.5.1. Particle size and zeta potential

The particle size and zeta potential of ELR-5TR1-pDNA were measured using a Zetasizer NanoZs (Malvern) at 37°C. The mean Z-average (nm), polydispersity index (PDI) and zeta potential (mV) were used for data analysis.

2.5.2. Transmission electron microscopy (TEM)

TEM measurements were performed using a JEOL JEM-1230 electron microscope operating at 120 kV. The polyplex solution was dropped onto carbon-coated copper grids and images recorded after drying for 4 hours at 37 °C.

2.6. Cell culture

Human breast cancer (MCF-7) and liver hepatocellular carcinoma (HepG2) cell lines were maintained in EMEM supplemented with 10% FBS, 2mM glutamine, 1% NEAA. Human fibroblasts (HFF-1) were cultured in DMEM supplemented with 15% FBS. Human breast cancer (SKBR3) cells were cultured in McCoy's 5A medium supplemented with 10% FBS. All complete media were supplemented with 100 U·mL⁻¹ penicillin and 0.1 mg·mL⁻¹ streptomycin. Cells were cultured in a humidified 5% CO₂

atmosphere at 37 °C, replacing the medium every two days. Cell lines were harvested at 70–80% confluence and were used between passages 2 and 6.

2.7. Transfection assays

2.7.1. Cell viability assay of polyplexes functionalized with aptamers

ELR-5TR1-pDNA polyplexes containing pCMV-Gaussia Luciferase plasmid were formed and their effect on cell viability assessed. Thus, MCF-7 cells were plated at a cell density of 3×10^4 cells per cm^2 and incubated overnight. They were then incubated with the ELR-5TR1-pDNA polyplexes formed with 1.7 nM pCMV-Gaussia Luciferase plasmid or 1 μL Turbofect, used as reference transfection polymer, under the same conditions for 5 hours in antibiotic- and FBS-free culture medium. After this time, the medium was replaced with complete medium and the cells were incubated for a further 43 h at 37 °C. Cells were visualized by contrast phase microscopy using a Leica SP5 confocal microscope (Leica Microsystems).

2.7.2. Analysis of transfection efficiency by Luciferase expression

A total of 3×10^4 cells per cm^2 of MCF-7, SKBR3 or HepG2 and 1×10^4 cells per cm^2 of HFF-1, in order to have the same level of confluence, were seeded onto 96-well plates and grown overnight. The cells were then incubated in an antibiotic- and serum-free medium for 5 h in the presence of the polyplexes (ELR-5TR1-pDhMUC1-luciferase); 1 μL of Turbofect and the nude plasmid DNA were used as control. The medium was then replaced by serum-containing medium and the cells cultured for a further 43 h. At this point, a 20 μL aliquot was removed from the culture medium and mixed with the luciferase substrate (Thermo Scientific, USA). The light produced was measured using a SpectraMax L luminometer (Molecular Devices, USA). The protein content of the lysate was determined by a Bradford assay using a SpectraMax M2e

microplate reader (Molecular Devices, USA). Luciferase expression is reported as relative light units (RLU) per mg total protein.

2.7.3. Cell transfection assays by cellular viability

96-Well plates seeded with 3×10^4 cells per cm^2 of MCF-7, or 1×10^4 cells per cm^2 of HFF-1, were incubated at 37 °C/5% CO_2 overnight prior to treatment with the polyplex. For these experiments, ELR-5TR1-pDhMUC1-ricin polyplexes containing different amounts of pDNA (1.7×10^{-3} , 1.7×10^{-2} , 1.7×10^{-1} and 1.7 nM) were formed and incubated with cells in an antibiotic- and serum-free medium at 37 °C/5% CO_2 for 5 h. After this time, the medium was replaced with fresh complete medium and the cells cultured for a further 43 h prior to analysis. Cell viability was quantified using the Alamar Blue® assay following the manufacturer's instructions and the fluorescence intensity (F.I.) of test samples and controls measured at an emission wavelength of 590 nm after excitation at 560 nm using a SpectraMax M2e microplate reader (Molecular Devices, USA). Cell viability was calculated as:

$$\% \text{ Cell viability} = 100 \times (\text{F.I. polyplex-treated cells} / \text{F.I. polymer-treated cells})$$

CC50, defined as the cytotoxic drug concentration lethal for 50% of cells, was calculated and considered as the pDhMUC1-ricin concentration at which 50% cell death was observed.

2.8. *In vivo* assays

The *in vivo* experimental protocols were performed in accordance with the recommendations of the Guideline for the Care and Use of Laboratory Animals and approved by the Ethics Committee from the University of Valladolid (Spain). Female Balb/c nu/nu mice aged 5-7 weeks and weighing about 17 g were purchased from Janvier Labs (France). 17β Estradiol pellets weighing 0.72 mg (Innovative Research of America, USA) were implanted in the loose skin of the mouse's mid-

scapular region after anesthetization with Vetflurane (Virbac, UK). Two days after implantation of the pellet, mice received a single subcutaneous xenograft injection of 1.0×10^6 MCF-7 cells suspended in 100 μ L of 1:1 minimum medium (Geltrex™ reduced growth factor basement membrane matrix, Gibco) into the right abdominal flank. Both tumor growth, measured by a caliper, and body weight were monitored daily throughout the experiment (23 days). Tumor volume was calculated using the formula $0.523 LW^2$ where L is the length and W the width of the tumor in mm. After seven days, once the mean tumor volume had reached 50 mm³, all mice were randomly separated into five statistical groups of eight animals each: group 1, placebo (5% glucose), group 2, negative control (70nM ELR-5TR1-pDhMUC1-luciferase, no therapeutic pDNA), and three groups treated with different doses of therapeutic plasmid ELR-5TR1-pDhMUC1-ricin (1.7, 17 and 70 nM). All doses were prepared with ELR-5TR1-pDNA at a final volume of 100 μ L in 5% glucose. Furthermore, a drug safety control group containing mice with no tumors treated with the maximum dose of ELR-5TR1-pDhMUC1-ricin (70 nM) and another drug safety control group (sham control) corresponding to animals injected with Geltrex matrix lacking tumor cells were included. Administration of the first treatment dose was considered as day 0. All treatments were administered peritumorally on days 0, 2, 4, 6 and 9. At day 23, the animals were sacrificed by manual cervical dislocation as indicated in the relevant regulations. After necropsy, tumors were extracted, weighed and properly stored.

2.9. Tissue Processing, histological staining and immunohistochemical assays

Tumors were fixed with 4% paraformaldehyde and embedded in paraffin. The paraffin tumor blocks were then serially sectioned into sections with a thickness of 5 μ m and transferred onto glass microscopy slides. Histological sections were subsequently de-paraffinized and re-hydrated for hematoxylin-eosin (H&E), Picro

Sirius and immunohistochemistry (IHC) staining. For IHC analysis of the sections, antigen retrieval was performed by incubation in 10 mM sodium citrate buffer pH 6 at 95°C for 20 min, then cooling for 20 min at room temperature. The sections were then washed and incubated in blocking solution (PBS supplemented with 2% BSA and 10% goat serum Invitrogen, ref 50-197Z) for 30 min at room temperature. The samples were incubated overnight at 4°C with the following primary antibodies: anti-MUC1 (1:100) (ref ab15481), anti-ki67 (1:500) (ref ab15580) and anti-CD31 (1:50) (ref ab28364) in antibody diluent (Dako). The slides were subsequently washed with PBS and then incubated with fluorescent secondary antibody Goat Anti-Rabbit (ref ab150077) at a 1:500 dilution in blocking buffer for 40 min at room temperature. Cell nuclei were counterstained with 4'-6-diamidino-2-phenylindole (DAPI) stain.

2.10. Statistical analysis

Results were expressed as mean \pm SD. The statistical significance of the results was analyzed using SPSS (version 20). The RLU/mg of ELR-pDNA polyplexes in transfection was analyzed using Student's t-test. All results with $p < 0.05$ for three independent experiments were considered to be statistically significant. In animal studies, differences between the mean tumor masses on the last day of treatment were compared using a one-way analysis of variance ANOVA (ANOVA, $\alpha = 0.05$, $p < 0.05$). Following ANOVA, a Tukey-Kramer post-hoc analysis was performed to compare the mean of one group with the mean of another group. A p value of less than 0.05 was considered to be statistically significant and is indicated in the corresponding figures with an asterisk, as reported in the results.

3. RESULTS

3.1. Design of pDhMUC1-ricin

The therapeutic plasmid DNA was based on the commercial pDhMUC1-luciferase plasmid, with the luciferase gene being replaced by the modified ricin gene containing the preprotrypsin leader (1698bp) in order to avoid difficulties in post-translational modifications of ricin, thus creating a new pDhMUC1-ricin (4403bp) (Figure S1 and S2). However, since N-t modifications have been shown to have important effects on protein expression, a small sequence of five amino acids from the original leader sequence was conserved to ensure expression of the holotoxin in mammalian cells. Thus, the luciferase gene pDhMUC1 (2705 bp) was excised from the plasmid using *NheI* and *NcoI* restriction enzymes (Figure S2A). In a parallel reaction, the inserted modified ricin gene (1698 bp) was released from the preprotrypsin plasmid by *PscI* and *NheI* digestion. After purification of the plasmid and insert, a ligation reaction led to creation of the new pDhMUC1-ricin. Cloning was confirmed by analyzing diagnostic digestion by *EcoRI* by agarose electrophoresis, which corroborated the plasmid construct size of 4403 bp, and by DNA sequencing, which confirmed the correctness of the sequence (Figure S2B). This pDhMUC1-ricin was used as therapeutic plasmid in suicide gene therapy experiments.

3.2 Synthesis and characterization of the ELR-5TR1

The ELR polymer corresponding to the amino acid sequence MESLLP (VPGKG)₇₂V was produced as described previously [31]. Endotoxins were eliminated and their levels evaluated, and were always found to be <1 EU/mg. Functionalization of the ELR with PEG-cyclooctyne was obtained via an amidation reaction between the ϵ amine group from the lysine present in one equivalent of ELR and 0.46 equivalents of the reactant NHS-cyclooctyne-PEG, which carries an activated carboxylic group as the *N*-succinimidyl ester (Figure S3). After lyophilization, a white spongy solid was obtained (92 mg, 2.83 μ mol) in a chemical yield of 91.6%. Due to the high molecular

weight of the ELR (32 kDa) in comparison with the low conversion required (2.1 mol of ELRx72:1 mol of PEG-cyclooctyne), which includes 217 Da for the PEG-cyclooctyne, it was not possible to quantify the amount of NHS-cyclooctyne-PEG incorporated using mass spectrometry as the weight of the latter falls within the margin of experimental error (0.5%). In the ^1H NMR spectrum, the appearance of new signals characteristic of the cyclooctyne derivative at 7.0 ppm (H-N from carbamate), 4.0 ppm (methylene group adjacent to carbamate and cyclopropyl group) and 2.9 ppm (methylene groups adjacent to the nitrogen of lysines forming the new amide bond) was observed (Figure S4). These signals allowed us to deduce that the PEG-cyclooctyne group was present along the peptide chain. Although the integration of these peaks was not sufficiently clear, it was possible to assign a conversion degree of 68% for the lysines based on the 7.0 ppm peak (this peak would integrate for 1.37H for 100% conversion, therefore the 0.93H obtained suggests a conversion of 68%).

Once the PEG had been bound to the ELR, a click reaction was performed between the ELR-PEG and azide-5TR1 with or without Cy5 (Figure S3). The 5TR1 aptamer labeled with Cy5 was used in a parallel reaction under the same conditions in order to verify the incorporation of aptamers into the ELR-PEG-cyclooctyne to form a polyplex by fluorescence and detect them by flow cytometry. For the click chemistry reaction, 1.1 equivalents of azide-5TR1 or azide-5TR1-Cy5 was mixed with 1 equivalent of modified ELR-PEG-cyclooctyne in aqueous solution at 4°C, as described in section 2.3.2. Incorporation of the 5TR1 aptamer was corroborated by gel retardation assay (EMSA), absorbance and flow cytometry (Figure S5, S6A and B). A solution of ELR-5TR1 biopolymer containing about 150 ng 5TR1 with 10% SDS was loaded onto a 3% Methaphor gel. As shown in Figure S5, the 5TR1 aptamer contained in the ELR-5TR1 construct was present and retained on the agarose gel, whereas 5TR1

alone was able to migrate freely along the gel. In addition, the concentration of 5TR1 in the ELR-5TR1 biopolymer was estimated by measuring the absorbance at 260 nm. As shown in Figure S6A, the absorbance of ELR-PEG-cyclooctyne used as control was almost zero due to the monotonous composition of the ELR, whereas it was around 0.62 AU₂₆₀ for ELR-PEG-5TR1, thus allowing us to quantify the amount of DNA. After the click reaction, 0.1 mmol of 5TR1 was coupled to 0.4 mmol of ELR-PEG-cyclooctyne with 92% substitution.

Once the biopolymer had been lyophilized, fluorescent polyplexes comprising ELR-5TR1-Cy5 and pDNA were formed and analyzed by flow cytometry. As shown in Figure S6B, a homogeneous population corresponding to these polyplexes was observed when side versus forward scatter was plotted. In addition, when the intensity count was plotted as a function of FL6 channel, a 100% labeling was observed for polyplexes comprising Cy5-labeled 5TR1 when compared with the polyplexes lacking the aptamer (Figure S6C) used as control. Hence, flow cytometry analysis showed both incorporation of the labeled 5TR1 aptamer into the ELR-PEG-cyclooctyne and the ability of this ELR-5TR1 biopolymer to form polyplexes in the presence of plasmid DNA.

3.3. Polyplex size, zeta potential and TEM

The size of the ELR-5TR1-pDNA polyplexes was determined by dynamic light scattering (DLS) in 5% glucose solution. The results showed a homogeneous polyplex population with a size of 146.7 ± 7.5 nm (Figure 1A) and a PDI of 0.13. The formation of spherical nanoparticles with a size of 135.5 ± 20 nm was corroborated by TEM microscopy (Figure 1B), with all polyplexes showing a rounded shape. In addition, the zeta potential was measured, with the value for ELR-5TR1-pDNA

polyplexes beings +35.1 mV, which increased to +40 mV in the absence of 5TR1, thus corroborating the presence of the conjugated aptamer.

3.4. In vitro transfection assays

The lack of cellular toxicity of the ELR has been reported previously [30]. Despite this, an additional comparison with a commercial non-viral gene-delivery system (Turbofect) was performed (Figure S7) and the biocompatibility of the ELR-5TR1 construct for the target MCF-7 cells was confirmed. In order to use this ELR-5TR1 as a delivery vector, its transfection ability was tested with pDhMUC1-luciferase. Thus, the tumor cell lines (MCF-7 MUC1 (+), SKBR3 MUC1 (+), HepG2 MUC1 (-)) and the primary cell line (HFF-1 MUC1 (-)) were transfected with the ELR-5TR1-pDhMUC1-luciferase polyplexes. As shown in Figure 2, luciferase expression did not show any significant variation when compared with cells treated with pDhMUC1-luciferase nude plasmid or polyplexes comprising ELR and ELR-5TR1 in HepG2 and HFF-1 cells. In contrast, a significant increase was observed for SKBR3 treated with ELR-5TR1 polyplexes when compared with those incubated with ELR polyplexes. The highest significant increase in transfection (nearly sixfold) was observed for MCF-7 treated with ELR-5TR1 polyplexes when compared with polyplexes lacking the aptamer. The expression level of luciferase in MCF-7 cells was also found to be significantly higher than when using Turbofect.

3.5. *In vitro* specific cytotoxicity of therapeutic polyplexes

In order to evaluate the effect of pDhMUC1-ricin plasmid on human breast cancer MCF-7 and human foreskin fibroblast HFF1 transfected cells, a cytotoxicity assay was performed using non-transfected cells as control, as indicated in the Materials and

Methods section (2.7.3). Four different plasmid concentrations were tested and, as shown in Figure 3, no cytotoxic effects were observed for the primary fibroblast cell cultures at any concentration. In contrast, dose-dependent cytotoxicity was observed for MCF-7 cells at a plasmid concentration of 1.7×10^{-2} nM. CC50, which is defined as the cytotoxic concentration of drug lethal for 50% of cells, was calculated and found to be 0.28 nM. This value was therefore used for the following *in vivo* experiments.

3.6. Suicide therapy *in vivo*

To confirm whether the observed *in vitro* anti-tumor therapeutic potency of pDhMUC1-ricin polyplexes translates to the *in vivo* scenario, they were tested in a human breast xenograft transplanted into a Balb/c nude mouse model. Human breast cancer tumors were induced in estradiol-supplemented female Balb/c nude mice by subcutaneous injection of MCF-7 cells into a commercial matrix-forming gel. Seven days after the xenograft injection, animals with an average palpable tumor size of 50 mm³, were divided into groups and treated with two negative control treatments and three different concentrations (1.7, 17 and 70 nM (0.027, 0.27 and 1.1 µg plasmid/g mouse)) of therapeutic pDhMUC1-ricin. Treatments were administered a further four times, as indicated by the arrows in Figure 5 A) Tumor volumes were estimated daily using a caliper in double-blind measurements.

Our results showed significant differences in tumor volume growth evolution between both the placebo and negative control (pDhMU1-luciferase) and the treated groups (Figure 4A). This difference was maintained over time, reaching very significant values from day 10 ($p < 0.05$) to the end of the experiment ($p < 0.001$; day 23 after first injection). At this time, placebo and negative control tumors reached an average volume of 273 ± 90.12 and 233 ± 122.97 mm³, respectively, whereas the 70 and 17 nM

treatment groups exhibited tumors of around $44 \pm 32.84 \text{ mm}^3$, thus representing a reduction of more than 80%.

At the end of experiment, the tumors were extracted and weighed. The average tumor weight for the treated groups was 55.42 ± 21.67 , 60 ± 35.21 and 85.12 ± 55.44 mg for 70, 17 and 1.7 nM doses, respectively, compared with 145.2 ± 19.61 mg for the placebo group and 142.67 ± 57 mg for the negative control group. The results are plotted in Figure 4B and show significant differences between negative controls and the 70 nM and 17 nM treatment groups. Despite this, the group treated with the 1.7 nM dose did not show any significant differences with respect to the placebo and negative control groups, thus suggesting that the treatment exhibits a dose-dependent pattern, which contrasts with the tumor volume results, where all doses produced a similar reduction (Figure 4). In addition, mice showed no adverse side effects, as reflected in the normal weight gain throughout whole experiment, the absence of anomalous behavior in all groups (Figure S8), and the lack of toxic symptoms in the drug safety control group.

A qualitative characterization of the tumors was carried out using both histological and immunohistochemical techniques. Thus, hematoxylin/eosin (H&E) and picro sirius staining (Figures 5 and 6, respectively) provided general information on the composition of the tumor.

Histological sections of representative tumors from the placebo and treated groups are shown in Figure 5. An abnormal solid mass comprising a tumor nucleus surrounded by connective tissue and vessels was found in almost all cases. This zone is more extended and shows a high cell density, as demonstrated by the more intense hematoxylin staining in the control tumors (Fig. 5A) compared to the treated ones.

The latter shrunk in a dose-dependent manner, and some tumors from the group treated with the highest dose showed a lower cell density (Fig. 5B). Interestingly, no substantial variation in the area of accessory tumor tissues (vascular and connective tissue) was observed in any of the groups analyzed. As such, the considerable difference in size between the tumors from the treated and nontreated groups is due to the extension of the inner mass. These results were also corroborated by Picro Sirius staining (figure 6), which enabled us to identify connective tissue (collagen I and III fibers stained red, cytoplasm and muscle fiber stained orange/yellow). In tumors from the group treated with the highest dose (Fig. 6B), the inner tumor mass looks smaller and richer in collagen than the control tumor group (Fig. 6A).

A molecular characterization of the tumor was carried out by immunohistochemistry, evaluating the presence of residual human MCF7 tumor cells by immunostaining against MUC1 antigen, which is overexpressed in the MCF7 breast carcinoma cell line (Fig. 7). All tumors containing a compact inner tumor mass showed in this zone an intense positive immunostaining with anti-MUC1, with this positivity being evident in the inner tumor mass of tumors from the placebo group (Fig 7A). In contrast, tumors treated with ricin polyplexes 70 nM showed very low or negative immunostaining (Fig. 7B).

Immunostaining against MUC1 antigen confirmed the specificity of the treatment by allowing a significant reduction in the number of target tumor cells. As such, administration of more doses of the ricin polyplexes could eliminate all residual tumor cells.

Another breast cancer prognostic parameter is cell proliferation rate, as measured using the Ki67 antibody, which recognizes a nuclear antigen specifically expressed in proliferating cells. Cell proliferation was found to be lower in all

treated tumor groups compared with controls, and was undetectable in some tumors from the group treated with the highest dose (Figure S9, S10).

Tumor vessels were labelled by CD31 immunostaining (Fig. 7), with positive staining being observed in the area surrounding the tumor nucleus and inside the tumor mass for both placebo (A) and ricin polyplex (B) groups. The number of blood vessels (as measured by CD31 staining) did not decrease as significantly post-treatment compared with control tumors. However, the latter showed a more infiltrative profile, with vessels penetrating to the most central part of the tumor nucleus.

4. DISCUSSION

Previous studies by our group have demonstrated the ability of polyplexes comprising ELR, absorbed MUC1 aptamers, and a therapeutic plasmid containing the PAP-S gene to target breast cancer cells and cause cellular death [31]. This study extends our work with this system and uses it to create a double safety-lock regulated device controlled by the presence of MUC1. Moreover, the main objective of this study is to destroy transfected and neighboring breast cancer cells using a modified ricin, thereby increasing the potential harm without damaging nontumor cells both *in vitro* and *in vivo*. The first lock arises due to the presence of the 5TR1 aptamer, which was attached to the ELR via a PEG spacer in order to facilitate binding between the aptamer and its target. PEG has commonly been used as spacer in targeted drug-delivery systems due to its high aqueous solubility, lack of toxicity and immunogenicity, and high flexibility, which allows PEGylation with no steric hindrance [51, 52]. The 5TR1 aptamer binds to the aberrantly hypoglycosylated MUC1 located on the breast cancer-cell surface. The second lock corresponds to the

hMUC1 promoter, which ensures expression of the cytotoxic ricin with the preprotrypsin leader only in MUC1 overexpressing cells [53, 54].

Functionalization of ELR with the 5TR1 aptamer, as shown in Figure S4, is possible due to the presence of SDS, which promotes the cleavage of hydrogen bonds in the secondary protein structure but not covalent bonds. Since our previous experience with click chemistry showed high levels of substitution [47], we can assume that most of the 5TR1 in ELR-PEG is linked to the polymer. Indeed, the concentration of 5TR1 in the biopolymer was quantified by measuring the absorbance at 260 nm, which allowed us to confirm a chemical yield of about 92% (Figure S5A). A retardation assay and spectrophotometry showed the presence of 5TR1 in the ELR-PEG but were unable to corroborate the presence of 5TR1 in their functional conformation as a polyplex. To that end, labeled 5TR1-Cy5 was used in a parallel click reaction as described previously. Subsequent flow cytometry data showed that 100% of polyplexes comprising ELR-PEG-5TR1-pDNA were labeled with Cy5 (Figure S5B), thus confirming the presence of the aptamer in every polyplex and the ability of ELR-PEG-5TR1 to form such structures in the presence of pDNA.

It has been widely reported that particle size has an effect on the internalization pathway. Thus, particles with a size of about 200 nm are known to be internalized via the endocytosis pathway, which may be beneficial for rapid entry into cells. In contrast, particles up to 10 μm gain cellular entry via phagocytosis [56, 57]. The polyplexes comprising ELR-PEG-5TR1-pDNA have a diameter of 190 ± 7.5 nm (Figure 2A) and a PDI of 0.13, which, according to the literature, makes them suitable for cellular transfection. The low PDI and the zeta potential of +35.1mV provide the high stability required for gene-delivery purposes. Similar zeta potentials were obtained in

a previous study that gave satisfactory cell transfection results [30]. Additionally, a positive surface charge favors the internalization of polyplexes via the negatively charged plasma membrane [57]. Further characterization by TEM helped us to confirm that the complexes formed well-defined polyplexes with a homogenous size and shape (Figure S5B). The differences in size between the two measurements were attributed to the experimental conditions (polyplexes are hydrated for DLS and dried for TEM).

The ideal gene-therapy device is one that attacks the tumor and stroma cells while maintaining healthy cells intact. MCF-7 human breast cancer cells have been shown to overexpress the MUC1 gene, which codifies for MUC1 glycoprotein [58]. Indeed, amplification of the MUC1 gene has been found in about 40% of breast cancers and significantly correlates with increases in MUC1 mRNA and protein levels [59]. The MUC1 C terminal (MUC1-C) subunit is involved in activating intracellular signaling pathways that result in activation of the MUC1 gene and its overexpression in breast cancer cells [60]. As such, we hypothesized that use of a plasmid containing the promoter, which is potentially activated in presence of MUC1, could allow genetic expression in the target human breast cancer MCF-7 cells only. Indeed, transfection assays with pDhMUC1-luciferase using three tumors and one primary cell line (Figure 3) confirmed this hypothesis. In the case of HepG2 and HFF-1 MUC1 (-), luciferase expression did not show any variation when comparing cells treated with ELR-PEG-5TR1 and ELR polyplexes. In contrast, a significant increase was observed in SKBR3 cells MUC1 (+), although this increase was lower than that observed in MCF-7 cells. This difference between the two MUC1 (+) cell lines supports the lower expression of MUC1 in SKBR3 reported in the literature [61, 62]. Consequently, the most significant results with hMUC1 promoter were obtained for MCF-7 cells transfected with ELR-

PEG-5TR1 polyplexes, with luciferase expression being nearly six times higher than for the control ELR lacking the aptamer, thereby confirming the specificity of the system. This finding correlates with our previous experience with cytomegalovirus promoter (CMV) and coated aptamers, which showed a similar increase in luciferase expression when the aptamer was present [30] and confirmed the initial hypothesis regarding the use of PEG as a spacer to improve binding to MUC1. In addition, it is important to note that luciferase expression for MCF-7 cells with the ELR-PEG-5TR1 biopolymer was significantly higher than that obtained with the commercial product Turbofect lacking the aptamer used as reference polymer.

Use of the ELR-PEG-5TR1-pDhMUC1-ricin system in suicide gene therapy was assessed *in vitro*. A cytotoxic effect was found in MCF-7 cells, with a CC50 of 0.28 nM. In contrast, little or no effect was observed for HFF-1 cells, which are the most representative cell type in connective tissue [63] at all concentrations of the therapeutic device tested. This cytotoxic effect for pDhMUC1-ricin is in agreement with the expected toxic effects of ricin [64], thus suggesting the expression of functional and active ricin. Despite lacking CC50 data in MCF-7 cells, according to the literature, the CC50 for monkey kidney Vero cells incubated for 20 h with ricin is 7.6×10^{-3} nM [65], which contrasts with value of 0.67 pM for HeLa cells [66] and 0.1 nM when myeloid U937 cells when incubated for 12 h [67], thus showing that ricin cytotoxicity depends on the cell line, probably due to the different composition of glycoproteins on the cellular surface and the internalization pathway. This explains the cytotoxic effects observed after transfection with ELR-PEG-5TR1-pDhMUC1-ricin system. Thus, once an MCF-7 cell has been transfected, ricin is expressed as preproricin with the preprotrypsin leader sequence at N-terminal. Subsequently, by way of a protein maturation process [68, 69], mature ricin is secreted into the culture medium via an

exocytosis process, thus leading to the bystander effect. Some of this mature ricin re-enters the endoplasmic reticulum, where RTA becomes active and translocates to the cytosol, subsequently exerting its action on the transfected cell. Once ricin has been secreted into the medium, Ricin B-chain (RTB) facilitates the translocation to neighboring cells, where RTA inhibits protein synthesis, thus leading to apoptosis and cell death [37, 38]. The CC50 value obtained was used in subsequent *in vivo* experiments, where the minimum concentration was above this value.

The double safety-lock device ELR-PEG-5TR1-pDhMUC1-ricin allows control over the cellular entry and expression of ricin, which is important *in vivo* due to the potent action of this toxin. Treatment of mice bearing breast tumors with ELR-PEG-5TR1-pDhMUC1-ricin decreased tumor volume growth by up to 85% in comparison with the placebo group (Figure 5A). In addition, significant differences were found between groups treated with the therapeutic agent up to day 10 after the first injection. Moreover, the *in vivo* cytotoxic effect at 1.7 nM correlates with the CC50 obtained at 0.28 nM *in vitro*. Bearing in mind the change from a 2D culture to a 3D tumor, where cell accessibility is more difficult for this *in vivo* assay, at least six times more of the 0.28 nM dose was administered in order to ensure the cytotoxicity of the system. Additionally, the reduction in tumor volume was confirmed by weighing the tumors post-necropsy which showed significant differences between placebo and negative control group (145.2 ± 19.61 and 142.67 ± 57 mg respectively) and mice treated with the higher (55.42 ± 21.67 mg) and medium doses (60 ± 35.21 mg). This effect was not appreciable in the group treated with the lowest dose, thus suggesting that the therapeutic effect of therapy is dose-dependent (Figure 5B).

Marked differences were also observed at the histological level. Thus, a comparison of tumors from the control and treated groups showed a selective and dose-

dependent reduction in tumor area as a result of treatment. Indeed, treatment acts in a specific and selective way on tumor cells, as demonstrated by evaluating the prognostic factors MUC 1 and Ki-67 by way of immunohistochemical assays. In contrast, treatment has no adverse effects on accessory structures, animal health and behavior, or in the post-mortem exploration.

The data obtained show the antitumor efficacy of the system in breast cancer, with the lack of visual toxic symptoms in the treated animals support its use as an efficient device for breast cancer gene therapy.

5. CONCLUSION

We have developed a double-lock device comprising the biopolymer ELR-PEG-5TR1 and the therapeutic agent pDhMUC1-ricin. Binding of 5TR1 to the ELR was achieved via click chemistry, and the resulting ELR-PEG-5TR1 was able to form stable polyplexes in the presence of pDNA with a suitable size for gene-delivery purposes. The aptamer present in the corona binds to a specific target in tumor cells (the transmembrane underglycosylated MUC1 glycoprotein), and selective overexpression of the toxin ricin gene exclusively inside human breast cancer cells is obtained due to the presence of the MUC promoter, which controls its expression. Moreover, this double-lock device is able to target breast cancer cells, internalizing and expressing the toxic ricin gene inside these cells. This system has shown promising results *in vivo*, thus providing direct proof that ELRs can be linked to aptamers for use in breast cancer suicide gene therapy. Most previous studies with ricin have been performed in immunotherapy with RTA or the holotoxin and blocking of the galactose binding sites [40]. To the best of our knowledge, this is the first time that the whole ricin gene has been transferred into target cells as part of suicide gene therapy in breast cancer. Indeed,

the results presented herein will form the basis of future studies into the non-viral ELR designed herein and the therapeutic plasmid-containing ricin.

Acknowledgments

The authors are grateful for financial support from the European Social Fund (ESF) and the European Regional Development Fund (ERDF), as well as funding from the EU (NMP-2014-646075), the MINECO (PCIN-2015-010, MAT2015-68901-R, MAT2016-79435-R and MAT2016-78903-R), the JCyL (project VA317P18), the CIBER-BBN, the JCyL and the Instituto de Salud Carlos III under the "Network Center of Regenerative Medicine and Cellular Therapy of Castilla and Leon". The authors would like to thank R. García for her technical assistance.

REFERENCES

- [1] I. Dagogo-Jack, A. T. Shaw. Tumour heterogeneity and resistance to cancer therapies. *Nat. Rev. Clin. Oncol.* 15 (2018) 81-94.
- [2] L. Naldini. Gene therapy returns to centre stage. *Nature.* 526 (2015) 351-60.
- [3] J. Kim, J. Kim, C. Jeong C, W.J. Kim. Synergistic nanomedicine by combined gene and photothermal therapy. *Adv. Drug Deliv. Rev.* 98 (2016) 99-112.
- [4] S.K. Das, M.E. Menezes, S. Bhatia, XY, Emdad L, Sarkar D, et al. Gene Therapies for Cancer: Strategies, Challenges and Successes. *J. Cell. Physiol.* 230 (2015) 259-71.
- [5] A.S. Asad, M.A. Moreno Ayala, M.F. Gottardo, C. Zuccato, A.J. Nicola Candia, F.A. Zanetti, et al. Viral gene therapy for breast cancer: progress and challenges. *Expert Opin. Biol. Ther.* 17 (2017) 945-59.
- [6] R.A. Castillo-Rodríguez, M.L. Arango-Rodríguez, L. Escobedo, D. Hernandez-Baltazar, A. Gompel, P. Forgez, et al. Suicide HSVtk Gene Delivery by Neurotensin-Polyplex Nanoparticles via the Bloodstream and GCV Treatment Specifically Inhibit the Growth of Human MDA-MB-231 Triple Negative Breast Cancer Tumors Xenografted in Athymic Mice. *PLOS One.* 9 (2014) e97151.

- [7] M. Trepel, J. Korbelen, E. Spies, M.B. Heckmann, A. Hunger, B. Fehse, et al. Treatment of multifocal breast cancer by systemic delivery of dual-targeted adeno-associated viral vectors. *Gene Ther.* 22 (2015) 848.
- [8] H. Kong, C. Liu, T. Zhu, Z. Huang, L. Yang, Q. Li. Effects of an adenoviral vector containing a suicide gene fusion on growth characteristics of breast cancer cells. *Mol. Med. Rep.* 10 (2014) 3227-32.
- [9] H. Kong, L. Tao, K. Qi, Y. Wang, Q. Li, J. Du, et al. Thymidine kinase/ganciclovir and cytosine deaminase/5-fluorocytosine suicide gene therapy-induced cell apoptosis in breast cancer cells. *Oncol. Rep.* 30 (2013) 1209-14.
- [10] A. Immonen, M. Vapalahti, K. Tyynela, H. Hurskainen, A. Sandmair, R. Vanninen, et al. AdvHSV-tk Gene Therapy with Intravenous Ganciclovir Improves Survival in Human Malignant Glioma: A Randomised, Controlled Study. *Mol. Ther.* 10 (2004) 967-72.
- [11] M.A. Zaimy, N. Saffarzadeh, A. Mohammadi, H. Pourghadamyari, P. Izadi, A. Sarli, et al. New methods in the diagnosis of cancer and gene therapy of cancer based on nanoparticles. *Cancer Gene Ther.* 24 (2017) 233–243.
- [12] H. Yin, R.L. Kanasty, A.A. Eltoukhy, A.J. Vegas, J.R. Dorkin, D.G. Anderson. Non-viral vectors for gene-based therapy. *Nat. Rev. Genet.* 15 (2014) 541-55.
- [13] P. Kesharwani, K. Paknikar. K. M., V. Gajbhiye. (Eds.). *Polymeric Nanoparticles as a Promising Tool for Anti-cancer Therapeutics.* Academic Press. (2019).
- [14] Z. Karjoo, X. Chen, A. Hatefi. Progress and problems with the use of suicide genes for targeted cancer therapy. *Adv. Drug Deliv. Rev.* 99 (2016);99 Part A:113-28.
- [15] E. Coccoa, S. Lopez, A. D. Santin, M. Scaltriti. Prevalence and role of HER2 mutations in cancer. *Pharmacol. Ther.* 199 (2019) 188-196
- [16] H. Garg, R. Salcedo, G. Trinchieri, R. Blumenthal. Improved nonviral cancer suicide gene therapy using survivin promoter-driven mutant Bax. *Cancer Gene Ther.* 17 (2009) 155-63.
- [17] E. Sadeqzadeh, F. Rahbarizadeh, D. Ahmadvand, M.J. Rasaee, L. Parhamifar, S.M. Moghimi . Combined MUC1-specific nanobody-tagged PEG-polyethylenimine polyplex targeting and transcriptional targeting of tBid transgene for directed killing of MUC1 over-expressing tumour cells. *J. Control. Release.* 156 (2011) 85-91.
- [18] S.S. Pinho, C.A. Reis. Glycosylation in cancer: mechanisms and clinical implications. *Nat. Rev. Cancer.* 15 (2015) 540-55.
- [19] S. Nath, P. Mukherjee. Trends MUC1: a multifaceted oncoprotein with a key role in cancer progression. *Mol Med.* 20 (2014) 332-42

- [20] H.J. Vaughan, J.J. Green, S.Y. Tzeng. Cancer-Targeting Nanoparticles for Combinatorial Nucleic Acid Delivery. *Adv Mater.* (2019) p. 1901081
- [21] J.C. Rodríguez-Cabello, F.J. Arias, M. Alonso M, A. Girotti. Elastin-like polypeptides in drug delivery. *Adv. Drug Deliv. Rev.* 97 (2016) 85-100.
- [22] C. Garcia-Arevalo, F.J. Bermejo-Martin, L. Rico, V. Iglesias, L. Martin, J.C. Rodriguez-Cabello, et al. Immunomodulatory nanoparticles from elastin-like recombinamers: single-molecules for tuberculosis vaccine development. *Mol. Pharm.* 10 (2013) 586-97.
- [23] I. Gonzalez de Torre, F. Wolf, M. Santos, L. Rongen, M. Alonso, S. Jockenhoevel et al. Elastin-like recombinamer-covered stents: Towards a fully biocompatible and non-thrombogenic device for cardiovascular diseases. *Acta Biomater.* 12 (2015) 146-55.
- [24] J.R. McDaniel, S.R Macewan, M. Dewhirst, A. Chilkoti. Doxorubicin-conjugated chimeric polypeptide nanoparticles that respond to mild hyperthermia. *J. Control. Release.* 159 (2012) 362-7.
- [25] T.H. Chen, Y. Bae, D.Y. Furgeson. Intelligent biosynthetic nanobiomaterials (IBNs) for hyperthermic gene delivery. *Pharm. Res.* 25 (2008) 683-91.
- [26] J.C. Rodriguez-Cabello, M.J. Piña, A. Ibanez-Fonseca, A. Fernandez-Colino, F.J. Arias. Nanotechnological Approaches to Therapeutic Delivery Using Elastin-Like Recombinamers. *Bioconjug. Chem.* 26 (2015) 1252-65.
- [27] J. Gonzalez-Valdivieso, A. Girotti, R. Muñoz, J.C. Rodriguez-Cabello, F.J. Arias. Self-assembling ELR-based nanoparticles as smart drug-delivery systems modulating cellular growth via Akt. *Biomacromolecules.* 5 (2019) 1996-2007.
- [28] A. Fernández-Colino, D. Quinteros, D. Allemandi, A. Girotti, S. Palma, F.J. Arias. Self-assembling Elastin-like hydrogels for timolol delivery: development of an ophthalmic formulation against glaucoma. *Mol. Pharm.* 14 (2017) 498-4508.
- [29] R. Costa, A. Girotti, M. Santos, F.J. Arias, J.F. Mano, J.C. Rodríguez-Cabello. Cellular Uptake of Multilayered Capsules Produced With Natural and Genetically Engineered Macromolecules. *Acta Biomater.* 10 (2014) 2653-2662.
- [30] M.J. Piña, S.M. Alex, F.J. Arias, M. Santos, J.C. Rodriguez-Cabello, R.R. Mannemcherril, et al. Elastin-like recombinamers with acquired functionalities for gene-delivery applications. *J. Biomed. Mater. Res. A.* 103 (2015) 3166-78.
- [31] M.J. Piña, A. Girotti, M. Santos, J.C. Rodríguez-Cabello, F.J. Arias. Biocompatible ELR-Based Polyplexes Coated with MUC1 Specific Aptamers and Targeted for Breast Cancer Gene Therapy. *Mol. Pharm.* 13 (2016) 795–808.
- [32] I.S Reynolds, M. Fichtner, D.A. McNamara, E.W Kay, J.H M. Prehn, J.P. Burk. Mucin glycoproteins block apoptosis; promote invasion, proliferation, and migration;

and cause chemoresistance through diverse pathways in epithelial cancers. *Cancer Metastasis Rev.* 38 (2019) 237-257.

[34] B. Akbari, S. Farajnia, S. Ahdi Khosroshahi, F. Safari, M. Yousefi, H. Dariushnejad, et al. Immunotoxins in cancer therapy: Review and update. *Int Rev Immunol.* 36 (2017) 207-19.

[35] F.I. Lamb, L.M. Roberts, J.M. Lord. Nucleotide sequence of cloned cDNA coding for preporicin. *Eur. J. Biochem.* 148 (1985) 265-70.

[36] Y. Endo, K. Mitsui, M. Motizuki, K. Tsurugi. The mechanism of action of ricin and related toxic lectins on eukaryotic ribosomes. The site and the characteristics of the modification in 28 S ribosomal RNA caused by the toxins. *J. Biol Chem.* 262 (1987) 5908-12.

[37] L.M. de Souza, L.P. de Carvalho, J. S. Araujo, E.J.T. de Melo, O.L.T. Machado. Cell toxicity by ricin and elucidation of mechanism of Ricin inactivation. *Int. J. Biol. Macromol.* 113 (2018) 821-828.

[38] N. Tyagi, M. Tyagi, M. Pachauri, P.C. Ghosh. Potential therapeutic applications of plant toxin-ricin in cancer: challenges and advances. *Tumor Biology.* 36 (2015) 8239-8246.

[39] N. Sowa-Rogozińska, H. Sominka, J. Nowakowska-Gołacka, K. Sandvig, M. Słomińska-Wojewódzka. Intracellular transport and cytotoxicity of the protein toxin ricin. *Toxins (Basel)* 11 (2019) p. 350.

[40] M. Słomińska-Wojewódzka, K. Sandvig. Ricin and Ricin-Containing Immunotoxins: Insights into Intracellular Transport and Mechanism of action in Vitro. *Antibodies.* 2 (2013) 236.

[41] A. Shapira, I. Benhar. Toxin-based therapeutic approaches. *Toxins (Basel).* 2 (2010) 2519-83.

[42] P. Jiao, J. Zhang, Y. Dong, D. Wei, Y. Ren. Construction and characterization of the recombinant immunotoxin RTA-4D5-KDEL targeting HER2/neu-positive cancer cells and locating the endoplasmic reticulum. *Appl. Microbiol. Biotechnol.* 102 (2018) 9585-9594.

[43] R. Díaz, V. Pallarès, O. Cano- Garrido, N. Serna, L. Sánchez- García, A. Falgàs, et al. Selective CXCR4+ Cancer Cell Targeting and Potent Antineoplastic Effect by a Nanostructured Version of Recombinant Ricin. *Small.* 14 (2018) p. 1800665.

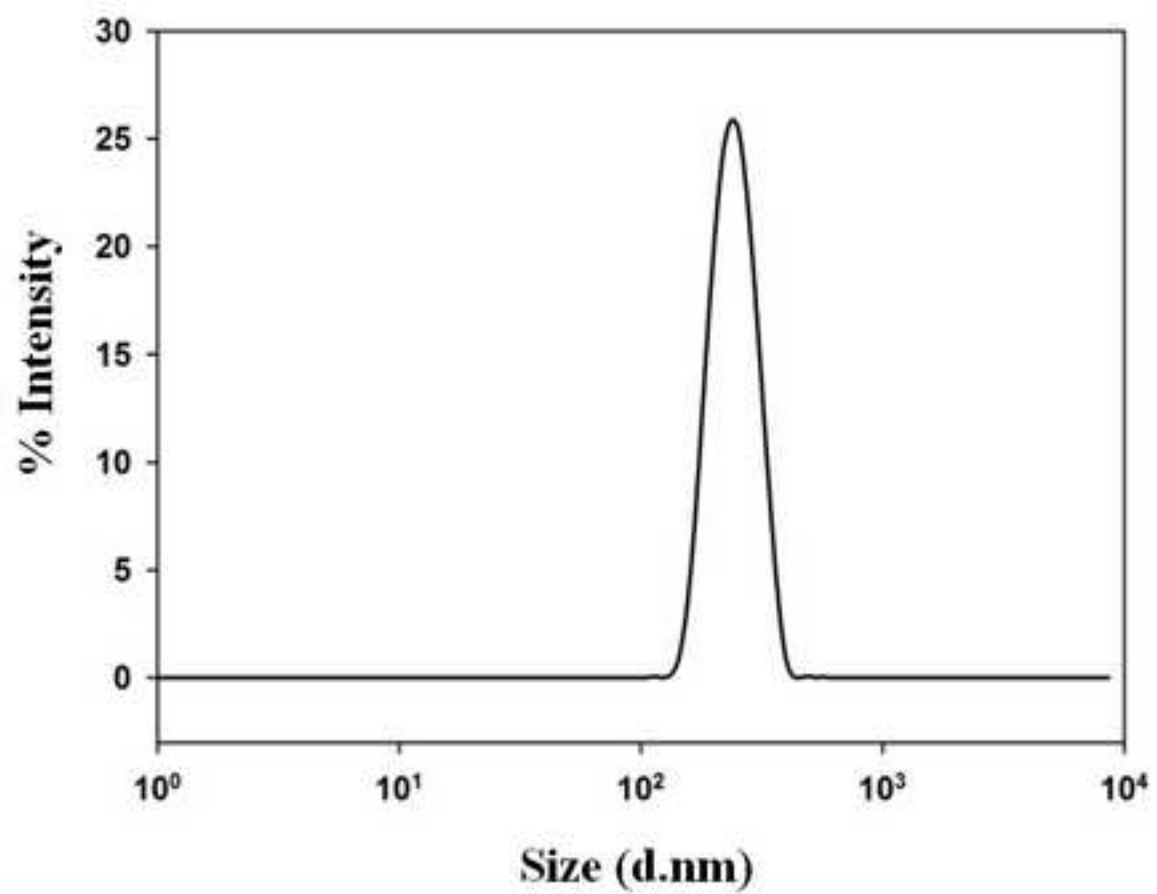
[44] B. Barriuso, P. Antolín, F.J. Arias, A. Girotti, P. Jiménez, M. Cordoba-Diaz, et al. Anti-Human Endoglin (hCD105) Immunotoxin Containing Recombinant Single Chain Ribosome-Inactivating Protein Musarmin 1. *Toxins.* 8 (2016) 184.

- [45] J. Schindler, S. Gajavelli, F. Ravandi, Y. Shen, S. Parekh, I. Braunchweig, et al. A phase I study of a combination of anti-CD19 and anti-CD22 immunotoxins (Combotox) in adult patients with refractory B-lineage acute lymphoblastic leukaemia. *Br. J. Haematol.* 154 (2011) 471-6.
- [46] S.K. Barta, Y. Zou, J. Schindler, N. Shenoy, T.D. Bhagat, U. Steidl, et al. Synergy of sequential administration of a deglycosylated ricin A chain-containing combined anti-CD19 and anti-CD22 immunotoxin (Combotox) and cytarabine in a murine model of advanced acute lymphoblastic leukemia. *Leuk. Lymphoma.* 53 (2012) 1999-2003.
- [47] I. González de Torre, M. Santos, L. Quintanilla, A. Testera, M. Alonso, J.C. Rodríguez Cabello. Elastin-like recombinamer catalyst-free click gels: Characterization of poroelastic and intrinsic viscoelastic properties. *Acta biomater.* 10 (2014) 2495-505.
- [48] S.H. Jalalian, M. Ramezani, K. Abnous, S.M. Taghdisi. Targeted co-delivery of epirubicin and NAS-24 aptamer to cancer cells using selenium nanoparticles for enhancing tumor response in vitro and in vivo. *Cancer Lett.* 416 (2018) 87-93
- [49] G. Zhou, G. Wilson, L. Hebbard, W. Duan, C. Liddle, J. George, L. Qiao. Aptamers: A promising chemical antibody for cancer therapy. *Oncotarget.* 7 (2016) p. 13446.
- [50] A. Shapira, I. Benhar. Toxin-Based Therapeutic Approaches. *Toxins.* 2 (2010) 2519-83.
- [51] Y. Patil, U. Toti, A. Khadair, L. Ma, J. Panyam. Single-Step Surface Functionalization of Polymeric Nanoparticles for Targeted Drug Delivery. *Biomaterials.* 30 (2009) 859-66.
- [52] S.S. Banerjee, N. Aher, R. Patil, J. Khandare. Poly(ethylene glycol)-Prodrug Conjugates: Concept, Design, and Applications. *J. Drug Deliv.* 2012 (2012) 17.
- [53] R. M. Tholey, S. Lal, M. Jimbo, R. A. Burkhart, F. F. Blanco, J. A. Cozzitorto, et al. MUC1 Promoter-Driven DTA as a Targeted Therapeutic Strategy against Pancreatic Cancer. *13* (2015) 439-448.
- [54] S. Xiang, P. Zou, J. Wu, F. Zheng, Q. Tang, J. Zhou, et al. Crosstalk of NF- κ B/P65 and LncRNA HOTAIR-Mediated Repression of MUC1 Expression Contribute to Synergistic Inhibition of Castration-Resistant Prostate Cancer by Polyphyllin 1-Enzalutamide Combination Treatment. *Cell. Physiol. Biochem.* 47 (2018) 59-773.
- [55] G. Sahay, D.Y. Alakhova, A.V. Kabanov. Endocytosis of nanomedicines. *J. Control. Release.* 145 (2010) 182-95.
- [56] W.L.L. Suen, Y. Chau. Size-dependent internalisation of folate- decorated nanoparticles via the pathways of clathrin and caveolae-mediated endocytosis in ARPE- 19 cells. *J. Pharm.* 66 (2014) 564-573.

- [57] M. Futami, Y. Watanabe, T. Asama, H. Murata, H. Tada, M. Kosaka, et al. Uniformly Cationized Protein Efficiently Reaches the Cytosol of Mammalian Cells. 23 (2012) 2025-2031.
- [58] T. M. Horm, J.A. Schroeder. MUC1 and metastatic cancer: expression, function and therapeutic targeting. *Cell Adh. Migr.* 7 (2013) 187-198.
- [59] E. Lacunza, M. Baudis, A.G. Colussi, A. Segal-Eiras, M.V. Croce, M.C. Abba. MUC1 oncogene amplification correlates with protein overexpression in invasive breast carcinoma cells. *Cancer Genet. Cytogenet.* 201 (2010) 102-10.
- [60] D.W. Kufe. MUC1-C oncoprotein as a target in breast cancer: activation of signaling pathways and therapeutic approaches. *Oncogene.* 32 (2013) 1073-81.
- [61] R. Singh, U. Samant, S. Hyland, P.R. Chaudhari, W.S. Wels, D. Bandyopadhyay. Target-specific cytotoxic activity of recombinant immunotoxin scFv(MUC1)-ETA on breast carcinoma cells and primary breast tumors. *Mol. Cancer Ther.* 6 (2007) 562-9.
- [62] M.D. Walsh, S.M. Luckie, M.C. Cummings, T.M. Antalis, M.A. McGuckin. Heterogeneity of MUC1 expression by human breast carcinoma cell lines in vivo and in vitro. *Breast Cancer Res. Treat.* 58 (1999) 255-66.
- [63] B. Alberts, A. Johnson, J. Lewis. *Biology of the Cell.* In: Science G, editor. 4th edition ed. New York. 2002.
- [64] L. Polito, M. Bortolotti, M.G. Battelli, G. Calafato, A. Bolognesi. Ricin: An Ancient Story for a Timeless Plant Toxin. *Toxins.* 11 (2019) p. 324.
- [65] D. Pauly, S. Worbs, S. Kirchner, O. Shatohina, M.B. Dorner, B.G. Dorner. Real-Time Cytotoxicity Assay for Rapid and Sensitive Detection of Ricin from Complex Matrices. *PLOS One.* 7 (2012) e35360.
- [66] J.M. Ferreras, L. Citores, R. Iglesias, P. Jiménez, T. Girbés. Use of Ribosome-Inactivating Proteins from Sambucus for the Construction of Immunotoxins and Conjugates for Cancer Therapy. *Toxins.* 3 (2011) 420-41.
- [67] S.K. Kochi, R.J. Collier. DNA Fragmentation and Cytolysis in U937 Cells Treated with Diphtheria Toxin or Other Inhibitors of Protein Synthesis. *Exp. Cell Res.* 208 (1993) 296-302.
- [68] R.G. Chubet, B.L. Brizzard. Vectors for expression and secretion of FLAG epitope-tagged proteins in mammalian cells. *Biotechniques.* 20 (1996) 136-41.
- [69] C.J. Guerriero, J.L. Brodsky. The Delicate Balance Between Secreted Protein Folding and Endoplasmic Reticulum-Associated Degradation in Human Physiology. *Physiol. Rev.* 92 (2012) 537-76.

Figure 1
[Click here to download high resolution image](#)

A



B

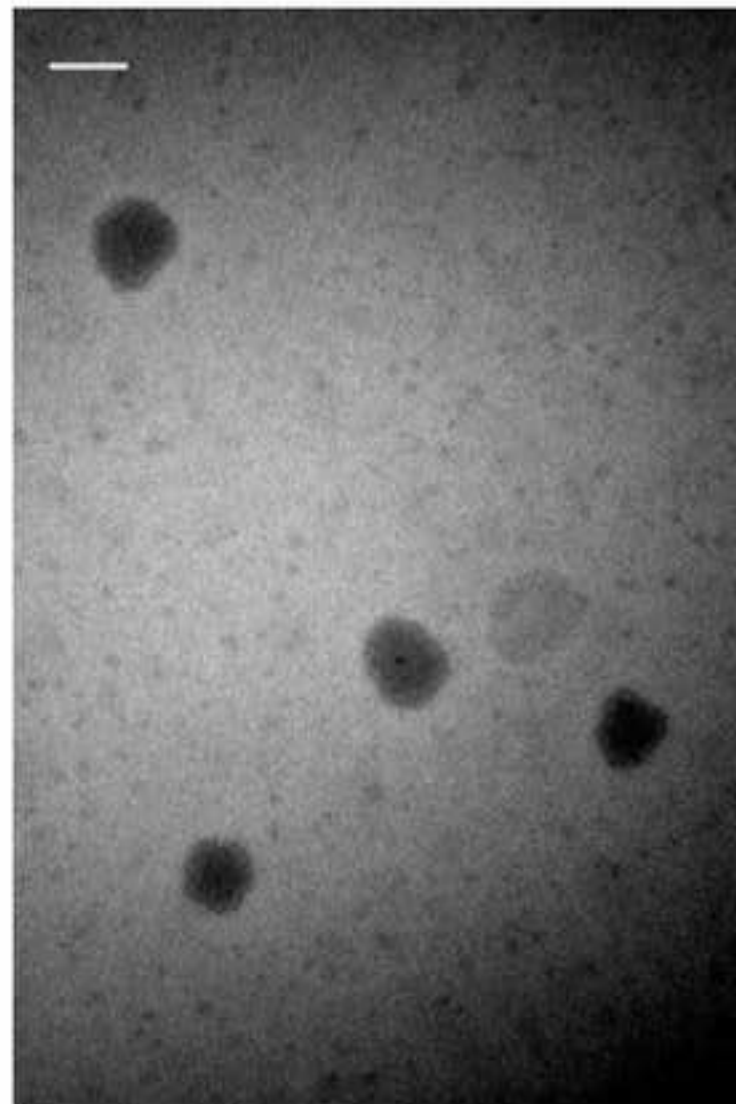


Figure 1. Polyplex size and morphology of ELR-5TR1-pDNA. (A) Graph showing the scattered light intensity (percent) as function of size (diameter, nm). (B) TEM image of polyplexes formed at a 50/1/4 N/P/P_{apt} (8500 ELR/1 pDNA/2000 5TR1) ratio. The scale bar corresponds to 100 nm.

Figure 2
[Click here to download high resolution image](#)

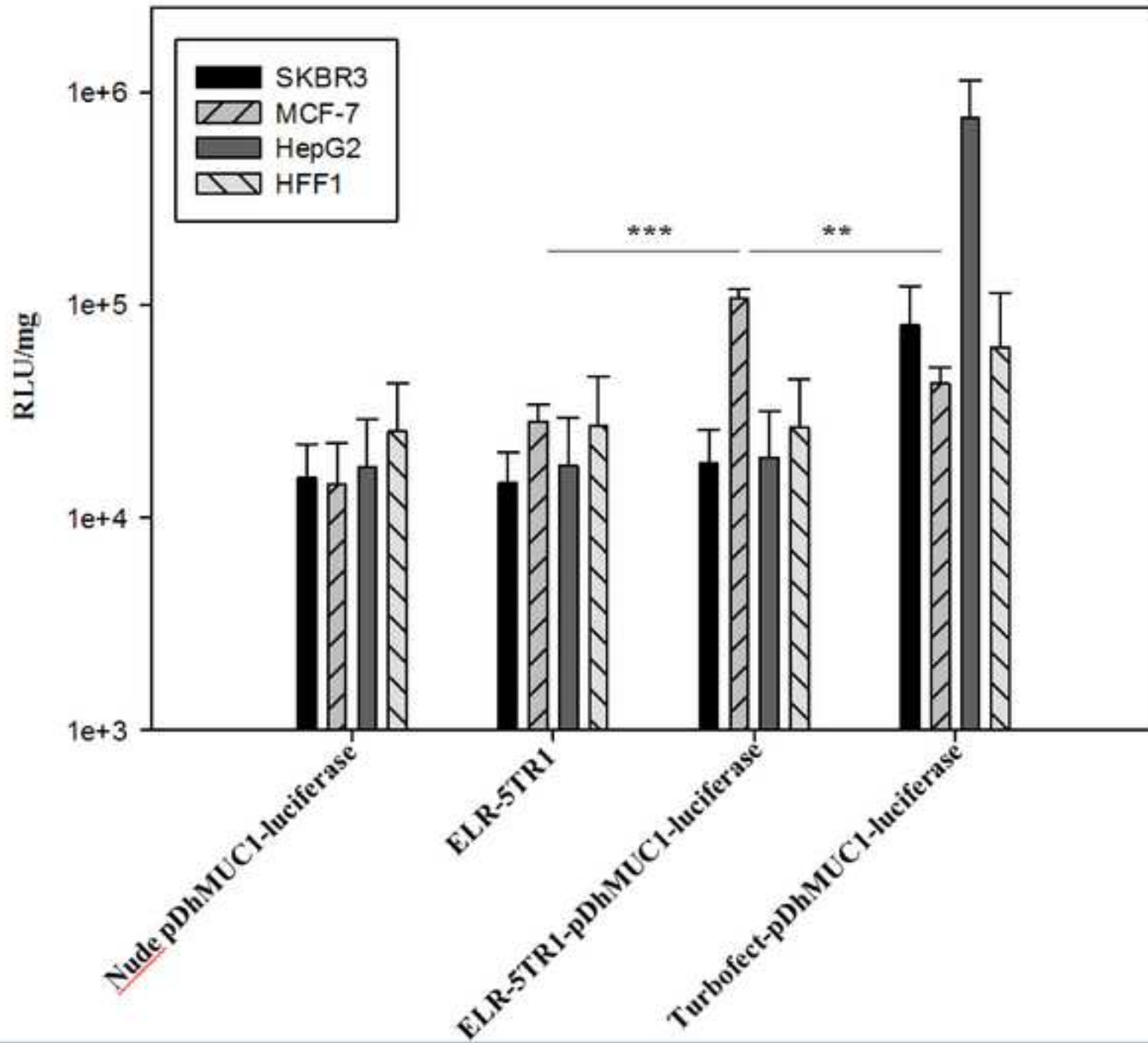


Figure 2. Luciferase expression by pDhMUC1-luciferase contained in ELR-5TR1- pDhMUC1-luciferase polyplexes. Nude pDhMUC1-luciferase and Turbofect-pDhMUC1-luciferase were used as negative and positive controls, respectively. ELR polyplexes were used as control for aptamer specificity. Luciferase activity is expressed in RLU/mg protein lysate. The results are expressed on a logarithmic scale as mean±standard error of three independent experiments. **: p<0.01, ***: p<0.001

Figure 3
[Click here to download high resolution image](#)

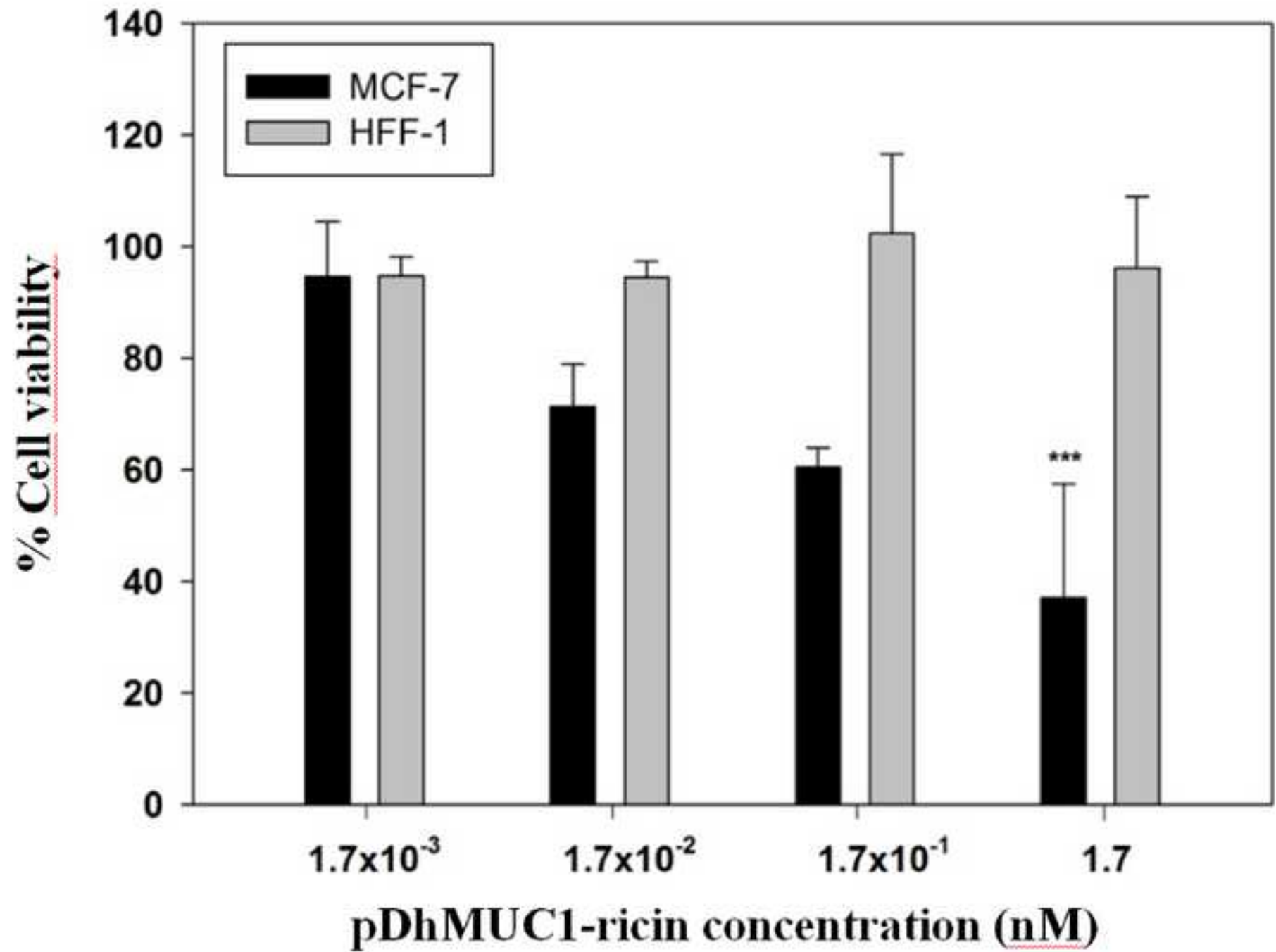


Figure 3 Cytotoxicity of pDhMUC1-ricin polyplexes for MCF-7 and HFF1 cells. Incubation with the transfectant polyplex was followed by 48 hours under standard culture conditions. These results are representative of three independent experiments, with four replicates in each experiment. Values are shown as mean +/- SD.

***: $p < 0.001$

Figure 4

[Click here to download high resolution image](#)

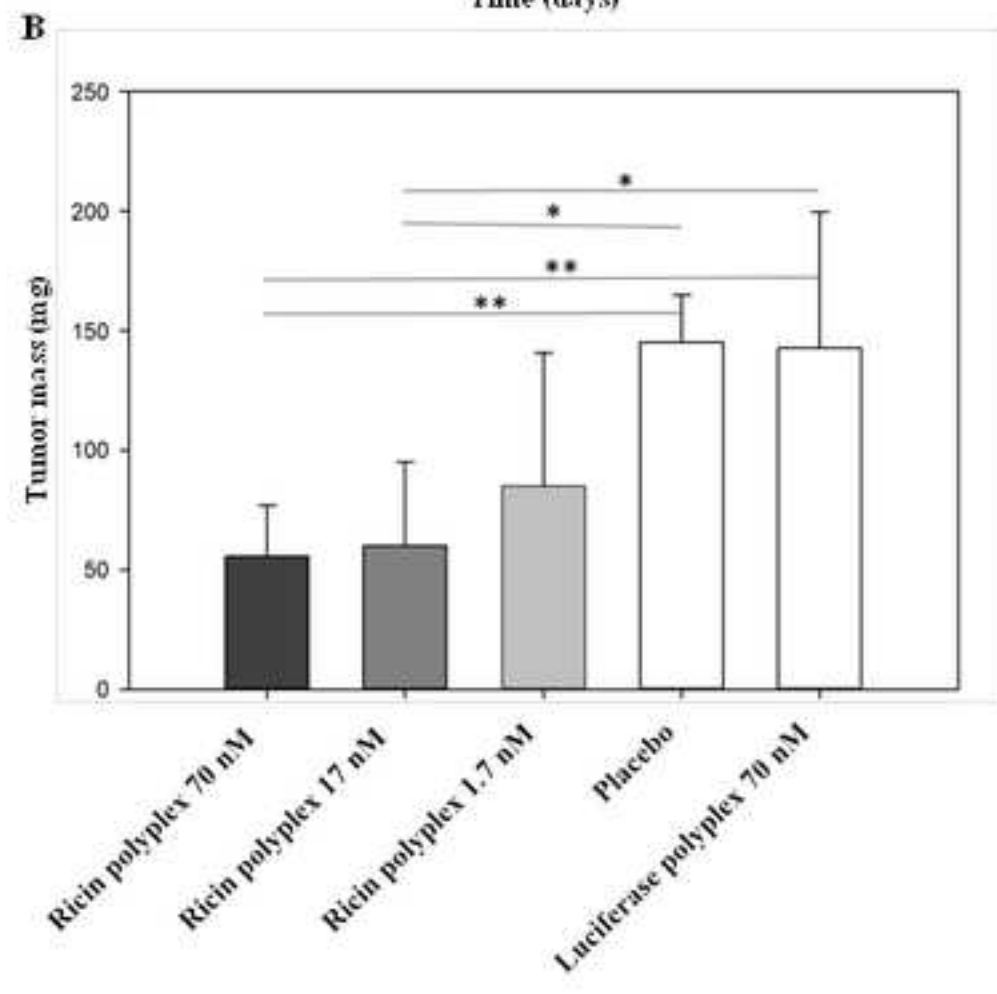
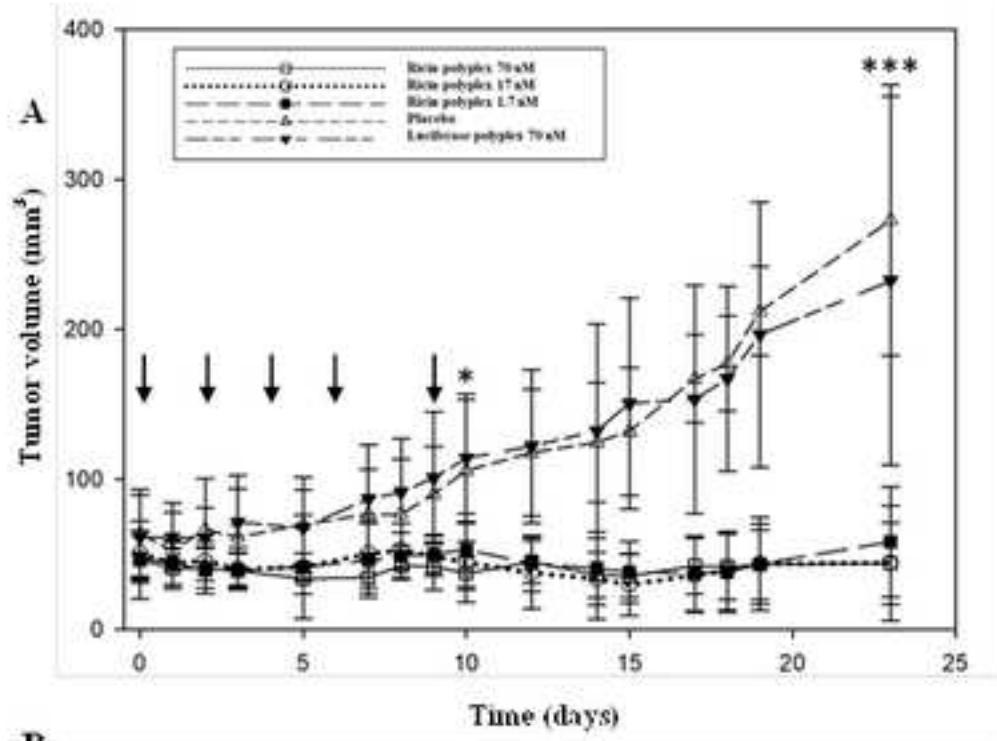


Figure 4. *In vivo* antitumor activity following treatment with ELR-5TR1-pDhMUC1-ricin complexes and negative controls. (A) Tumor volume evolution during 23 days after five injections of placebo, luciferase polyplex 70 nM control group, 1.7, 17 and 70 nM of therapeutic plasmid and 70 nM of pDhMUC1-luciferase. Arrows indicate the injections of treatments. (B) Tumor mass evaluation after necropsy. Data represent the mean \pm S.D. A statistical analysis showed significant differences (*: $p < 0.05$, **: $p < 0.01$, ***: $p < 0.001$).

Figure 5
[Click here to download high resolution image](#)

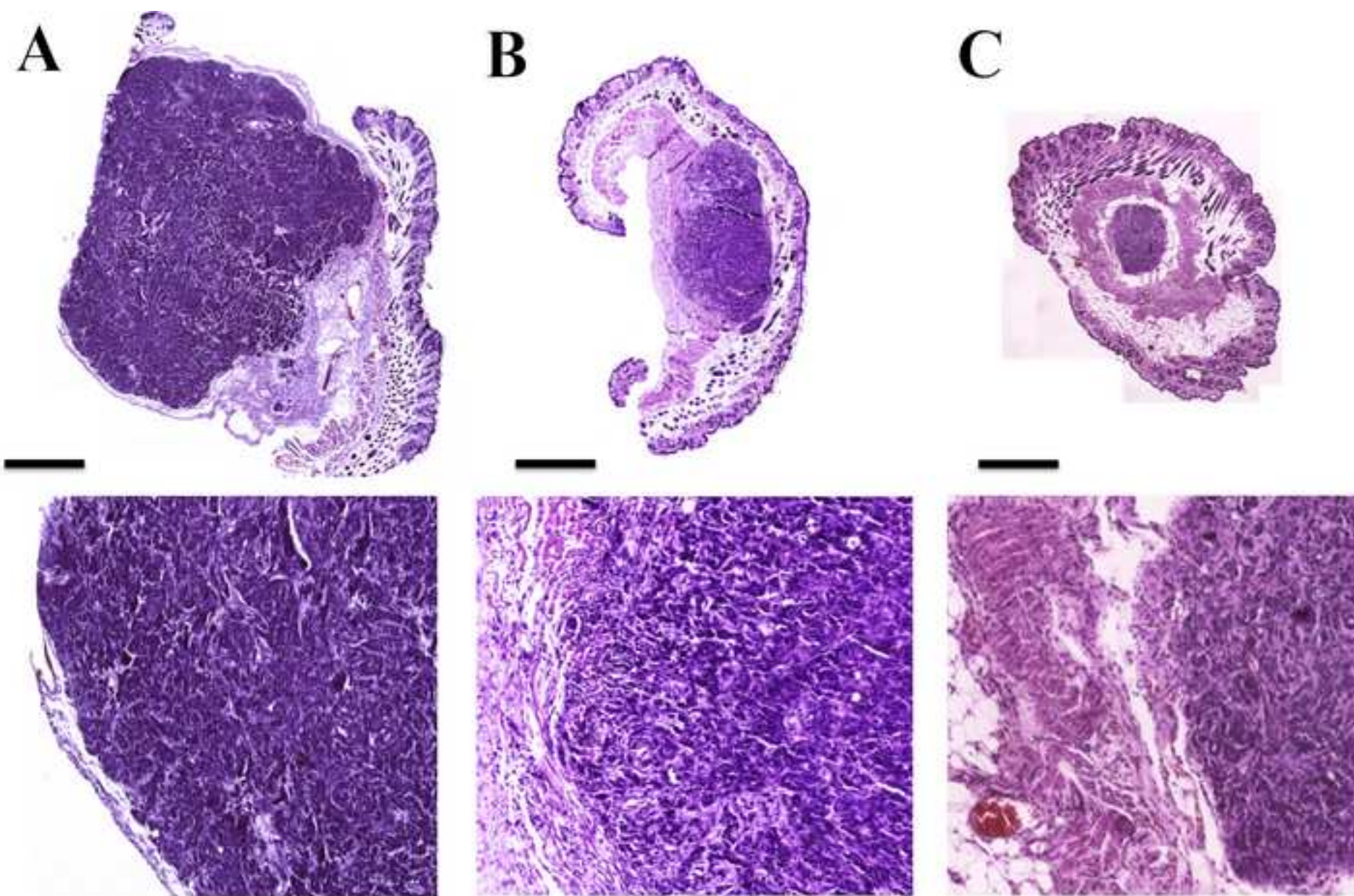


Figure 5. Microphotographs showing histological staining of tumors with hematoxylin-eosin (H&E) stain. The columns contain photographs of histological sections: A control tumor; B 1.7 nM and C 70 nM treatment dose. Scale bar:1000 micrometers

Figure 6
[Click here to download high resolution image](#)

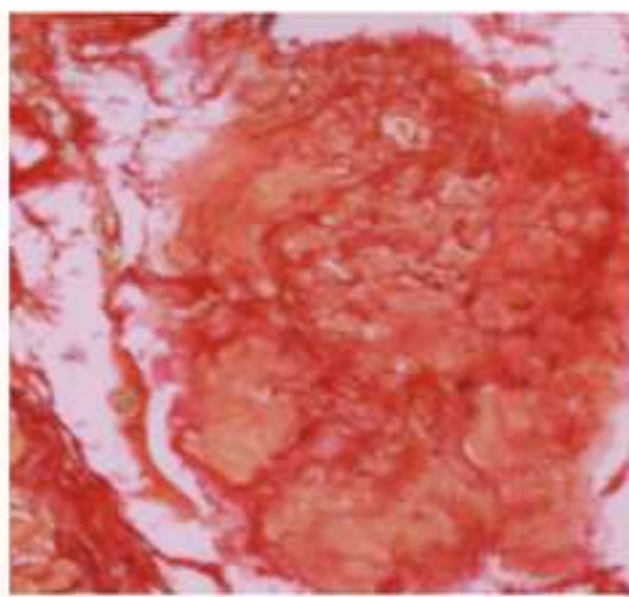
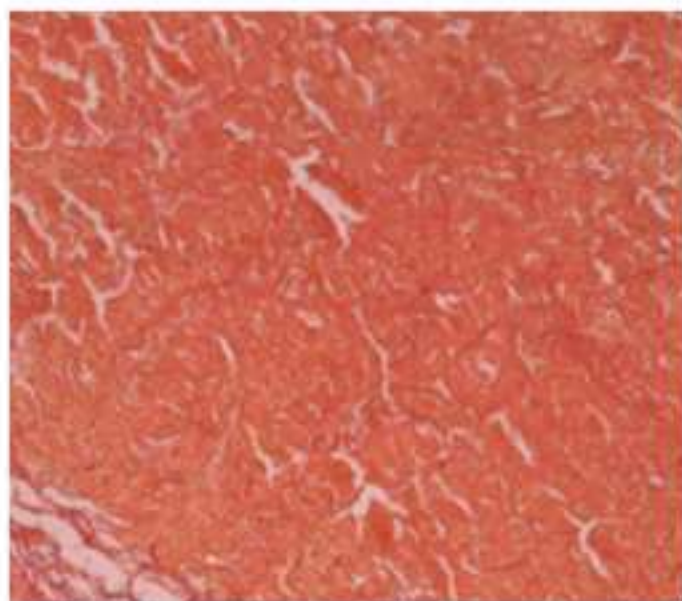
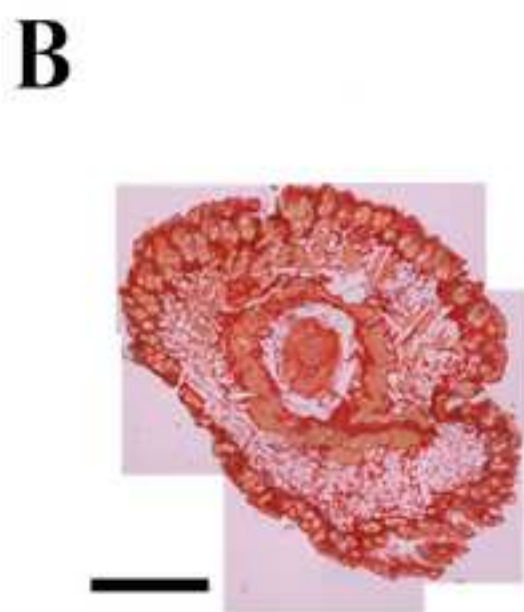
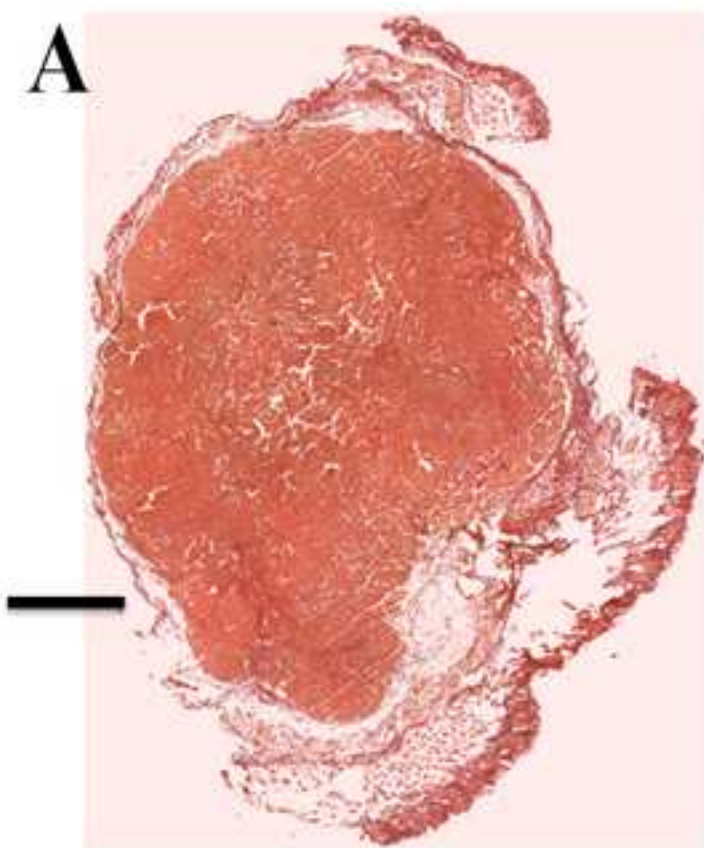


Figure 6. Microphotographs showing histological Picro red staining of tumors.

A: control and B: 70 nM treated tumors and sections thereof. Scale bar: 1000 micrometers.

Figure 7

[Click here to download high resolution image](#)

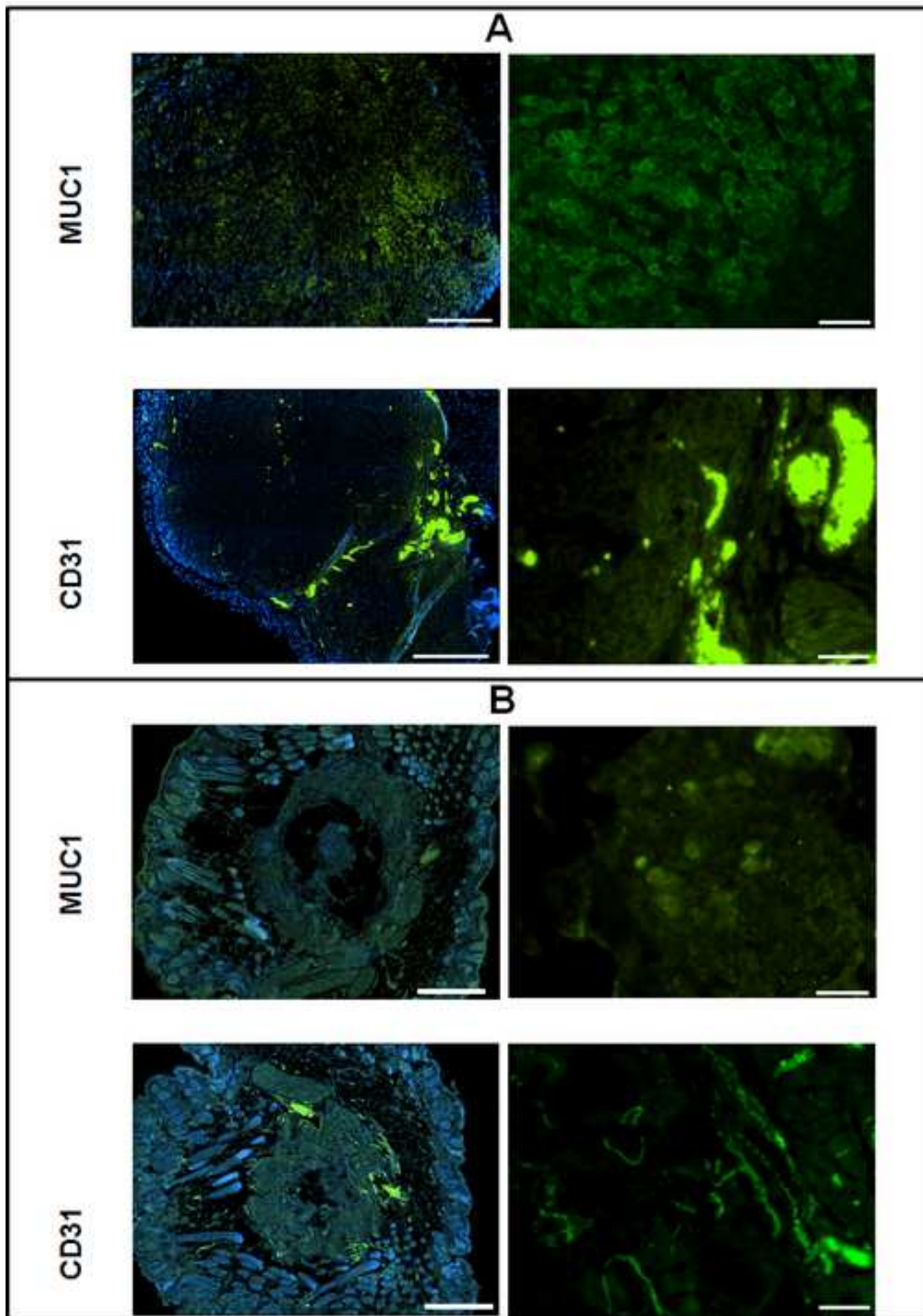


Figure 7. Expression of tumor and vascularization markers characterization. Immunohistochemistry was performed with specific antibodies against MUC1 or CD31 (immunofluorescence staining green) then stained with nuclear marker DAPI (blue). Photographs of the tumor (left) and sections thereof (right). In the sections is shown only the IHC staining to appreciate better IHC signals. Panel A: placebo, panel B: 70 nM dose treated group. Scale bar of tumors: 1000 micrometers, sections: 100 micrometers.

Supporting Information

[Click here to download Supplementary File: Supporting Information.docx](#)

Conflict of interest

The authors declare no competing financial interest.

DATA AVAILABILITY

The raw/processed data required to reproduce these findings cannot be shared at this time as the data also forms part of an ongoing study.

